RESEARCH MEMORANDUM

EXPERIMENTAL INVESTIGATION OF DRAG OF AFTERBODIES WITH EXITING JET AT HIGH SUBSONIC MACH NUMBERS

By Reino J. Salmi

Lewis Flight Propulsion Laboratory
Cleveland, Ohio

NATIONAL ADVISORY COMMITTEE
FOR AERONAUTICS
WASHINGTON
November 29, 1954

NACA RM E54I13

NATIONAL ADVISORY COMMITTEE FOR AERONAUTICS

RESEARCH MEMORANDUM

EXPERIMENTAL INVESTIGATION OF DRAG OF AFTERBODIES WITH EXITING JET AT HIGH SUBSONIC MACH NUMBERS

By Reino J. Salmi

SUMMARY

A small-scale experimental investigation was conducted to determine the pressure drag of various blunt-based conical afterbodies at Mach numbers from 0.6 to 0.9. A generalized series of bodies was included which incorporated convergent nozzles discharging unheated jets at various pressures from the base. In addition, ejector installations in both fuselage- and nacelle-type bodies were included which simulated subsonic cruise operation of nozzles designed for supersonic flight.

The results indicated that the external pressure drag of a blunt-based body of revolution with no jet was considerably reduced by boattailing. With a 5.6° boattail angle, the greatest drag reduction occurred when the base-to-body diameter ratio was reduced from 1.0 to 0.7. With a base-to-body diameter ratio of 0.525, the minimum pressure drag occurred between boattail angles of 8° and 10°.

When a convergent nozzle having a diameter of 0.375 that of the body discharged a jet from the base, boattailing was again effective in reducing the afterbody drag. With no boattail, the effect of the jet was to aspirate the large annular base to very low pressures. On a small base annulus the jet effects were generally favorable. The incorporation of a boattail, therefore, combined the favorable effects of reducing the base annulus and converging the flow before separation at the base.

In simulated ejector installations with a closed secondary shroud, it was found that the pressure drag of the high-angle shroud flaps could be very large in nacelle-type installations with no boattail upstream of the flaps. In a fuselage-type installation with an appreciable boattail ahead of the flaps, the drag of the closed flaps was greatly reduced. The effect of secondary flow on the external pressure drag of the ejector nozzles was small.

INTRODUCTION

The advent of sustained supersonic flight has brought renewed interest in the high subsonic speed range as a cruising point for both subsonic and supersonic aircraft. One of the aerodynamic problems in this speed range for which little information is presently available is that of afterbody design. With jet propulsion the problem is complicated by the interference effects of the jet on the flow over the afterbody. In addition, some severe fairing problems are encountered, particularly in the case of an aircraft with jet-engine afterburner inoperative and the nozzle-exit area reduced to the cruise condition.

The present small-scale investigation was designed to define the severity of the afterbody drag problems and to indicate relatively good design practice for the high subsonic Mach number range. Tests were made at nominal Mach numbers from about 0.6 to 0.9 on conical afterbodies with a convergent nozzle exiting at the base and having various base sizes and boattail angles. Also studied was a series of ejector configurations that simulated some of the afterburner-off conditions that may be encountered in nacelle and fuselage installations.

SYMBOLS

The following symbols are used in this report:

A	area
a_a	velocity of sound at stagnation conditions
C_D	pressure drag coefficient, $-\int_{r_n/r_{max}}^{1.0} C_p \, d\,(r/r_{max})^2 + \Delta C_D$
ΔC_D	tunnel-wall correction to measured drag coefficient
$C_{D,net}$	$-\int_0^{1.0} C_p \, d(r/r_{max})^2 + \frac{M_n(V_0 - V_n)}{q_0 A_{max}} + \Delta C_D$
C_p	pressure coefficient, $(p - p_0)/q_0$
D	diameter, in.
H	total pressure
M	Mach number

[redacted]

m	mass flow
$m_{n,2}/m_0$	ratio of bleed mass flow through jet exit to mass flow of free-stream tube of equal area
p	static pressure
q	dynamic pressure, $\gamma pM^2/2$
r	radius
T	total temperature
V	velocity
β	boattail angle, deg
γ	ratio of specific heats
δ	boundary-layer thickness
θ	secondary-nozzle flap angle, deg

Subscripts:

b	base
max	maximum
n	nozzle
p	primary
s	secondary
t	free wind tunnel
0	free stream

APPARATUS AND PROCEDURE

Tunnel

The test facility was a closed-wall circular wind tunnel 17.5 inches in diameter. As shown by figures 1 and 2, the tunnel consisted of a wooden bellmouth that contracted to a 20-inch-long steel cylindrical test section. Atmospheric air was discharged through the tunnel into the subsonic diffuser section of the 18- by 18-inch supersonic wind tunnel.

The tunnel speed was controlled by choking the downstream gate valve in the diffuser. With the gate valve wide open, the tunnel choked at the exit of the steel test section and the Mach number in the test area was 0.92. Probe surveys across the tunnel showed that uniform Mach number profiles existed across the tunnel sections where the afterbodies were tested. The longitudinal Mach number variation in the tunnel was determined from static-pressure orifices on the tunnel wall located at 3-inch intervals. In general, the longitudinal Mach number variation in the test section was small except near the exit at the highest Mach numbers, but these sections were well downstream of the test area. The free-stream Mach number was based on static pressures measured by a tunnel-wall orifice located just upstream of the afterbodies. The tunnel-wall and model pressures were recorded photographically from multitube manometers using tetrabromoethane as the fluid.

Models

The models consisted of a series of conical afterbodies mounted to a long cylindrical tube that projected into the tunnel through the bellmouth. As shown in figure 3, the configurations included (a) a general series and (b) an ejector series. The general series of afterbody shapes varied in base size and boattail angle and had a 0.75-inch-diameter convergent nozzle exiting at the base. The ejector series included three nacelle-type installations where simulated secondary-nozzle flaps were closed at angles of 30° (F), 45° (E), and 90° (D) with no boattailing ahead of the base, and three fuselage-type installations that incorporated an 8.46° boattail ahead of the base.

In the experimental investigation of tunnel-wall interference effects, two smaller models were used that were similar to one of the general series models, as indicated in figure 3. These models had diameters of 1.00 and 1.25 inches, which, together with the 2.00-inch-diameter model, provided a series of similar models having blockage values (A_{max}/A_t) of 0.33, 0.51, and 1.31 percent. High-pressure air (unheated) was supplied to the nozzles through the mounting tube; and, in the case of the ejectors, concentric tubes were used which allowed the two air flows to be controlled independently. The total pressure of the air to the convergent nozzles and to the primary nozzles of the ejector configurations was measured with a rake located in the mounting tube just ahead of the nozzle. The mass flow was calculated from the pressure and an assumed nozzle flow coefficient of 1. A rotameter was used to measure the mass flow of the secondary air. The temperatures of the primary and secondary air were measured with thermocouples located in the supply tubes. Static-pressure orifices were provided on the boattail and base of the models.

Tests were conducted at nominal Mach numbers ranging from about 0.6 to 0.9 with the corresponding free-stream Reynolds numbers varying from about 3.68×10^6 to 4.62×10^6 per foot. The static-temperature drop in the

tunnel at a Mach number of 0.9 was sufficient to cause supersaturation of the air that would be drawn in during periods of precipitation. No discrepancies in the data were evident, however, from operation during such conditions.

The boundary-layer thickness near the base of a 2-inch-diameter body was measured. The ratio of the boundary-layer thickness to the model diameter (δ/D_{max}) was approximately 0.17.

Tunnel-Wall Corrections

The present model and wind-tunnel setup is unique in that the model represents a body of such length that the flow over the cylindrical portion of the body preceding the base or afterbody boattail is substantially at uniform free-stream conditions. For this case the inviscid incompressible pressure distribution over the boattail integrates to a net force of zero if the wind-tunnel walls are at an infinite distance from the body. With the tunnel walls at a finite distance from the body, as in the present case, the cross-sectional area of the flow passage between the model and the tunnel walls increases as the flow progresses over the boattail. This results in a diffusion of the stream flow that would not occur in free flight. The increase in the static pressure accompanying the diffusion modifies the potential-flow boattail pressure distribution in such a way as to result in an apparent thrust force on the afterbody. Despite the small model size in the present tests, the interference to the condition of zero net force is appreciable at high subsonic speeds where the Mach number varies rapidly with flow area.

In order to approximate the correction for the potential-flow tunnel-wall interference, the flow was considered to be one-dimensional and isentropic. The thrust force on the body was calculated by the momentum theorem as equal to the change in momentum of the stream in diffusing from the annular flow area just upstream of the boattail to the flow area just downstream of the boattail. For the solid afterbody, the area just downstream of the boattail was the total cross-sectional area of the test section, while the presence of a jet reduced this area by the amount of the nozzle-exit area. The expression for the thrust or negative drag increment so derived is

$$\Delta C_D = 2\left(\frac{A_t}{A_{max}} - 1\right)\left(1 - \frac{\left(\frac{V}{a_a}\right)_2}{\left(\frac{V}{a_a}\right)_1}\right) + \frac{2}{\gamma M_1^2}\left(\frac{A_t}{A_{max}} - \frac{A_n}{A_{max}}\right)\left(1 - \frac{\left(\frac{p}{H}\right)_2}{\left(\frac{p}{H}\right)_1}\right)$$

where the subscripts 1 and 2 refer to the stations ahead of and just behind the boattail.

[redacted]

In a real fluid with the tunnel walls at infinity, the boattail pressure drag coefficient will not be zero because of viscous distortion of the potential-flow field. In applying the wall interference correction to the experimental data, it is assumed that (1) the local viscous effects on the afterbody do not influence the correction due to diffusion of the stream flow in the annular passage, and (2) the additional adverse pressure gradient on the boattail due to this diffusion does not appreciably influence the boattail boundary-layer growth and separation and hence the true drag coefficient.

The theoretical corrections so derived are presented in figure 4 for the two body diameters of interest herein and for a range of nozzle-exit sizes. The correction increases with Mach number and model size, and at Mach number 0.9 is relatively large for the 2-inch-diameter models. An indication of the adequacy of the method used is given in figure 5, where the variation with jet pressure ratio of the drag of three different sizes of geometrically similar models is presented. The uncorrected data show a large-scale effect, most of which is eliminated by the correction, which appears unaffected by jet pressure ratio. The variation in jet shape due to jet pressure ratio and mixing did not influence the calculation for wall-interference effects. The method was not considered accurate enough to warrant point-by-point correction to the pressure distributions. In addition, where discontinuities occur such as with blunt bases, the correction might be expected to be too large, since with separated flow the afterbody may not experience the full pressure rise. The conventional wake blockage correction was in the present case calculated to be small relative to the corrections applied and was not included.

RESULTS AND DISCUSSION

Afterbodies without Jet

Effect of boattailing on pressure drag. - The effects of boattailing on the external pressure drag coefficient of the conical afterbodies are shown in figure 6 for the jet-off case (equivalent solid body). The base pressure coefficients are assumed to apply over the entire base, and the tunnel-interference corrections applied were for the full pressure rise ($A_n = 0$). Figure 6(a) shows that, with a constant boattail angle of 5.63°, increasing the boattail length by reducing the base size resulted in a large drag reduction for base-to-body diameter ratios between 1.0 and 0.7. Similar results were obtained in free-flight tests reported in reference 1. Figure 6(b) indicates that, with a base-to-body diameter ratio of 0.525, the optimum boattail angle at transonic speeds is about 10°. This is somewhat higher than the optimum boattail angle for this speed range reported in reference 1. The drag coefficient for zero boattail angle in figure 6(b) was obtained by assuming the same base pressure coefficient as was measured for the model with a base-to-body diameter ratio of 1.0.

[redacted]

Effect of base bleed. - The effects of base bleed on the base pressure coefficient and on the drag coefficient are shown in figure 7. Significant reductions in the pressure drag coefficient were gained from the base bleed. The largest drag reduction resulted for the afterbodies with the largest bases, although the corresponding increase in the base pres- coefficient was the least. These results are in qualitative agreement with base bleed effects at supersonic speeds reported in reference 2. The net drag coefficient obtained when the momentum loss of the bleed air is considered is also indicated in figure 7 as $C_{D,net}$. The bleed air is assumed initially to have the free-stream momentum. In all cases the loss in momentum was greater than the decrease in the external pressure drag, indicating that the net drag is increased if free-stream air is taken in for the sole purpose of base bleed. The possibility of utilizing cooling air, which must be discharged somewhere, or boundary-layer air with reduced initial momentum remains, however.

Afterbodies with Jet

The pressure distributions over the general series of afterbodies with and without jet flow are shown in figure 8. The pressure distributions over the conical afterbodies are characterized by a low-pressure region of flow acceleration about the initial boattail break and a diffusion to higher pressures near the base, depending on the boattail length. The pressures over the downstream portions of the boattails indicate the possibility of separation ahead of the base. As the boattail length was increased by reducing the base-to-body diameter ratio at a constant boattail angle, the pressure at the rear of the body and the base pressure both increased. When the boattail angle was increased, the pressures around the initial boattail break decreased further, but the pressure recovery over the rear portion of the boattail increased and resulted in a decrease in the drag coefficient with increasing boattail angle up to the optimum boattail angle. The jet influenced the afterbody pressures mainly on the base and the boattail area just ahead of the base. For small base annuli, the jet increased the base and boattail pressures; but, for large base annuli, the pressures were decreased. On a small base annulus the jet may deflect the free-stream flow outward and thus decelerate the flow in the region of the base and increase the base pressure. For a large base the jet boundary can return to an axial direction before meeting the external flow; and, thus, the deflection of the free stream by the jet is small, and the jet aspirating effect on the semidead-air region reduces the base pressure.

The integrated pressure drag coefficients are presented in figure 9 as a function of the jet pressure ratio. The variations in the drag coefficient with jet pressure ratio are as would be expected after

examining the pressure distribution curves. The drag coefficient increased rapidly with jet pressure ratio for the afterbody with no boattailing, but for the body with the smallest base annulus the jet effects were small and generally favorable. Figure 10, which shows the effect of the jet on the drag of afterbodies with various boattail angles, indicates that the variation of the drag coefficient with jet pressure ratio is little affected by the boattail angle.

Ejector afterbody configurations. - The nacelle-type ejector configurations are characterized by the fact that they exhibit no boattailing ahead of the base formed by the simulated closed secondary-nozzle flaps. Such configurations exhibited large drag coefficients at practical operating jet pressure ratios (fig. 11). The drag coefficient at a jet pressure ratio of 3 may be of the order of 10 to 15 percent of conventional jet-engine thrust in the cruise condition. Reducing the secondary-nozzle flap angle from 90° to 30° was only moderately effective in reducing the large values of the drag coefficient. Figure 12, which shows the radial pressure distribution over the flaps, indicates that the flap pressures were fairly uniform.

As may be expected from the results obtained from the conical afterbodies, the fuselage-type ejector configurations, which had a fairly long boattail of 8.46° ahead of the base, exhibited relatively low drag coefficients and little effect of the jet at practical jet pressure ratios (fig. 13). The increment in drag due to closing the simulated secondary-shroud flaps 45° was small. As indicated by the pressure distribution curves in figure 14, the pressure recovered rapidly to higher than ambient values after the low-pressure peak caused by the flow around the initial boattail break. The boundary layer, therefore, experienced an adverse pressure gradient and may have been separated or near separation as it approached the base. The separation-type boundary-layer profile has low velocity or low shear at the wall compared with a fully developed flat-plate profile (as experienced with the nacelle at the point of forced separation); and, hence, the flow is less able to aspirate the base pressure to low values. This may in part explain why the pressures over the secondary-shroud flaps remained high. Comparison of the short-shroud ejector configuration is in this case difficult, because the pressures in the large annular base region were not obtained.

The drag coefficients of the nacelle- and the fuselage-type afterbodies are compared in figure 15 on the basis of equal primary-nozzle areas. It is significant that the drag of the fuselage-type afterbodies is considerably less than that of the nacelle-type afterbodies, even though the resulting fuselage body diameter is about 50 percent greater. In order to determine whether the drag of a body can be reduced by increasing the body diameter to obtain the benefits of boattailing, the forebody and friction drag would have to be considered.

[redacted]

Effect of secondary flow. - In the subsonic cruising range of jet pressure ratios, the external pressure drag coefficient was relatively little affected by secondary-air flows of about 7 percent of the primary (fig. 16). When the afterburner cooling passage forms a base annulus that is not closed for the cruise conditions, the secondary flow will increase the static pressure in the plane of the annulus. However, if the secondary air is taken in from the free stream solely for this purpose, a net increase in drag will result because of the momentum loss of the secondary air, as discussed in reference 3, for example.

SUMMARY OF RESULTS

The results of the investigation of the external pressure drag of various conical afterbody configurations at high subsonic Mach numbers can be summarized as follows:

1. The afterbody pressure drag of a blunt-based body of revolution was considerably reduced by decreasing the base-to-body diameter ratio from 1.0 to 0.7 with a 5.6° boattail. With a base-to-body diameter ratio of 0.525, minimum pressure drag was obtained with a boattail angle of approximately 10°.

2. When a convergent nozzle having a diameter 0.375 that of the body discharged a jet from the base, boattailing was again very effective in reducing the afterbody drag. With no boattail the effect of the jet and stream was to aspirate the large annular base to a very low pressure. The jet effects were generally favorable for small base annuli. The incorporation of a boattail combined the favorable effects of reducing the base annulus and of converging the flow before separation, which increased the afterbody and base pressures.

3. In simulated ejector installations with a closed secondary shroud, the pressure drag of the high-angle shroud flaps could be very large in nacelle-type installations with no boattail upstream of the flaps. In a fuselage-type installation with an appreciable boattail ahead of the flaps, the drag of the closed flaps was greatly reduced.

4. The effect on external drag of secondary flow in ejector nozzles was small.

Lewis Flight Propulsion Laboratory
National Advisory Committee for Aeronautics
Cleveland, Ohio September 22, 1954

REFERENCES

1. Stoney, William E., Jr.: Some Experimental Effects of Afterbody Shape on the Zero-Lift Drag of Bodies for Mach Numbers Between 0.8 and 1.3. NACA RM L53I01, 1953.

2. Cortright, Edgar M., Jr., and Schroeder, Albert H.: Investigation at Mach Number of 1.91 of Side and Base Pressure Distributions over Conical Boattails without and with Jet Flow Issuing from Base. NACA RM E51F26, 1951.

3. Vargo, Donald J.: Effects of Secondary-Air Flow on Annular Base Force of a Supersonic Airplane. NACA RM E54G28, 1954.

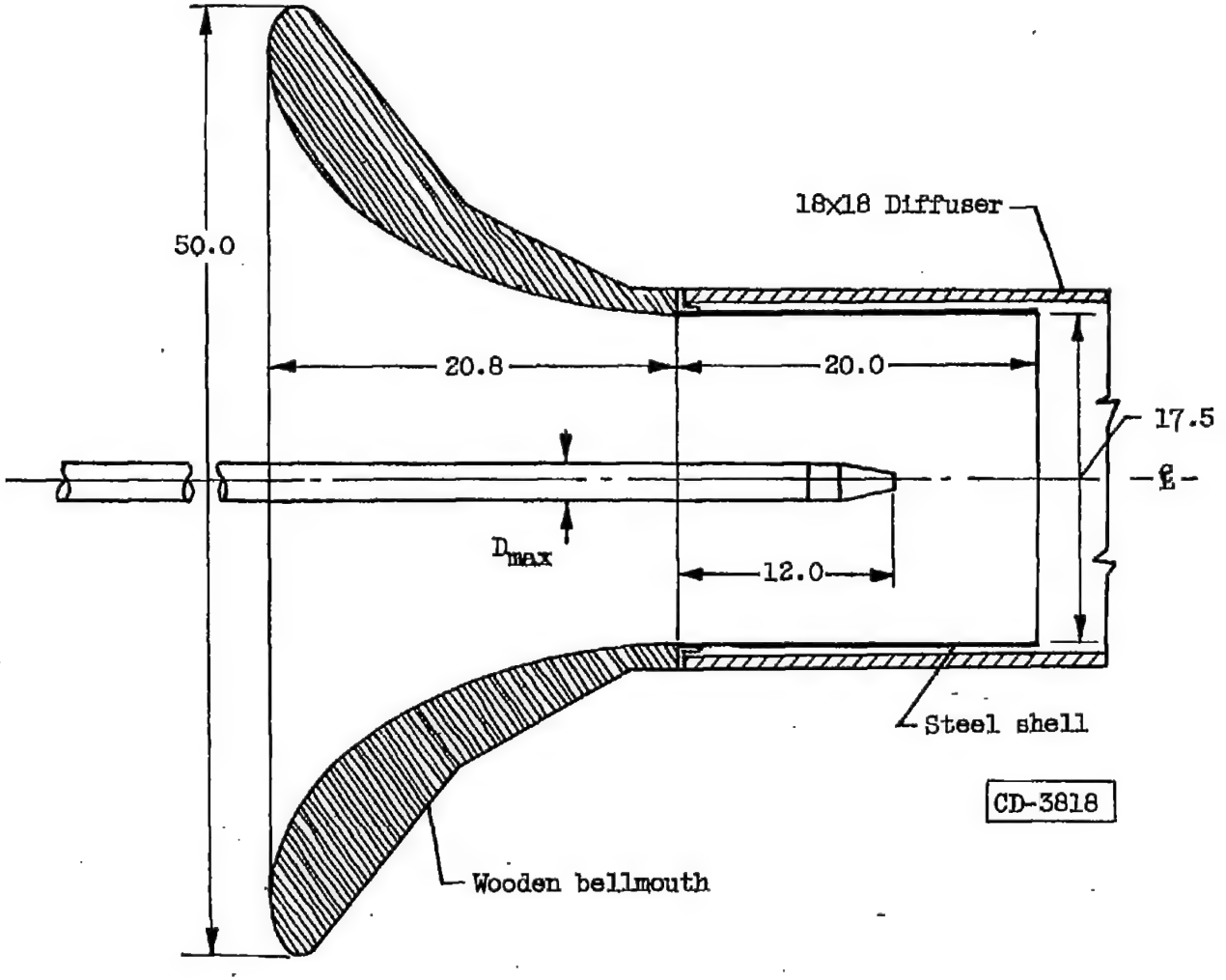

Figure 1. - Schematic diagram of tunnel and model. (All dimensions in inches.)

(a) Model in tunnel.

Figure 2. - Photograph of subsonic tunnel with model installed.

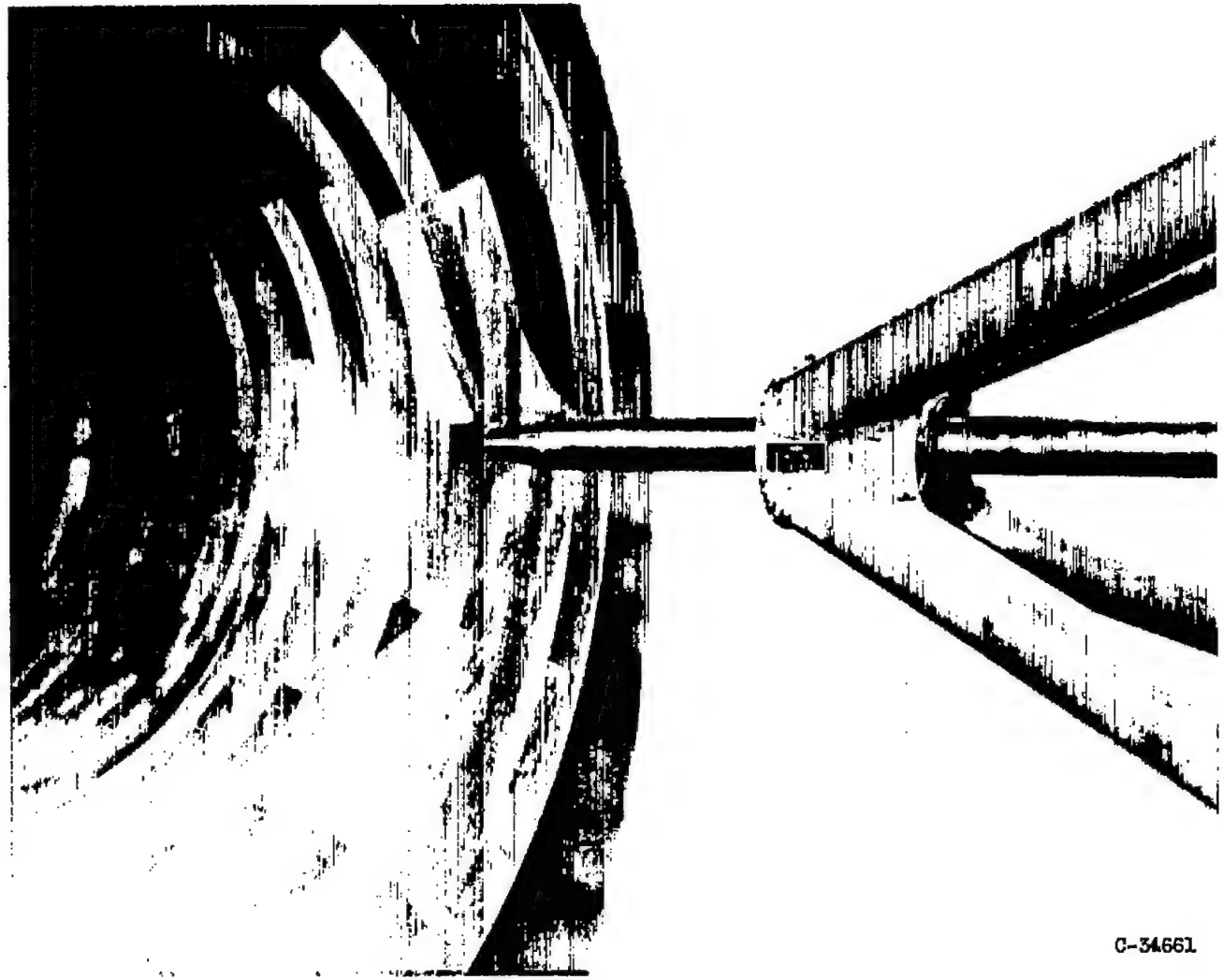

(b) Model withdrawn.

Figure 2. - Concluded. Photograph of subsonic tunnel with model installed.

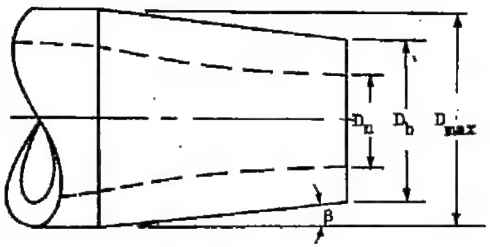

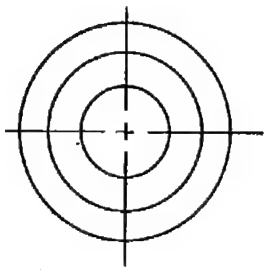

D_{max} = 2.00 in. D_n = 0.750 in.

D_b, in.	β, deg	D_b/D_{max}	D_b/D_n
0.835	5.63	0.418	1.11
1.050	5.63	.575	1.40
1.250	5.63	.625	1.67
1.500	5.63	.750	2.00
2.000	----	1.000	2.67
1.050	9.53*	.525*	1.40*
1.050	11.00	.525	1.40

*Also parameters for interference models (D_{max} = 1.25, 1.00).

(a) General series.

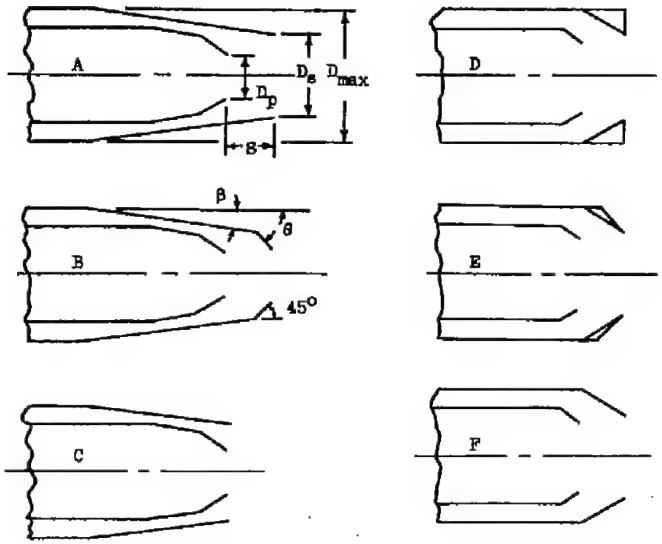

Fuselage installations

Nacelle installations

D_{max} = 1.250 in.

	D_p, in.	D_s, in.	s, in.	β, deg	θ, deg
A	0.474	0.714	0.518	8.46	0
B	.474	.485	.518	8.46	45
C	.474	.850	.065	8.46	0
D	.710	.775	.485	0	90
E	.710	.775	.485	0	45
F	.710	.775	.485	0	30

(b) Ejector series.

Figure 3. - Geometry of afterbody configurations.

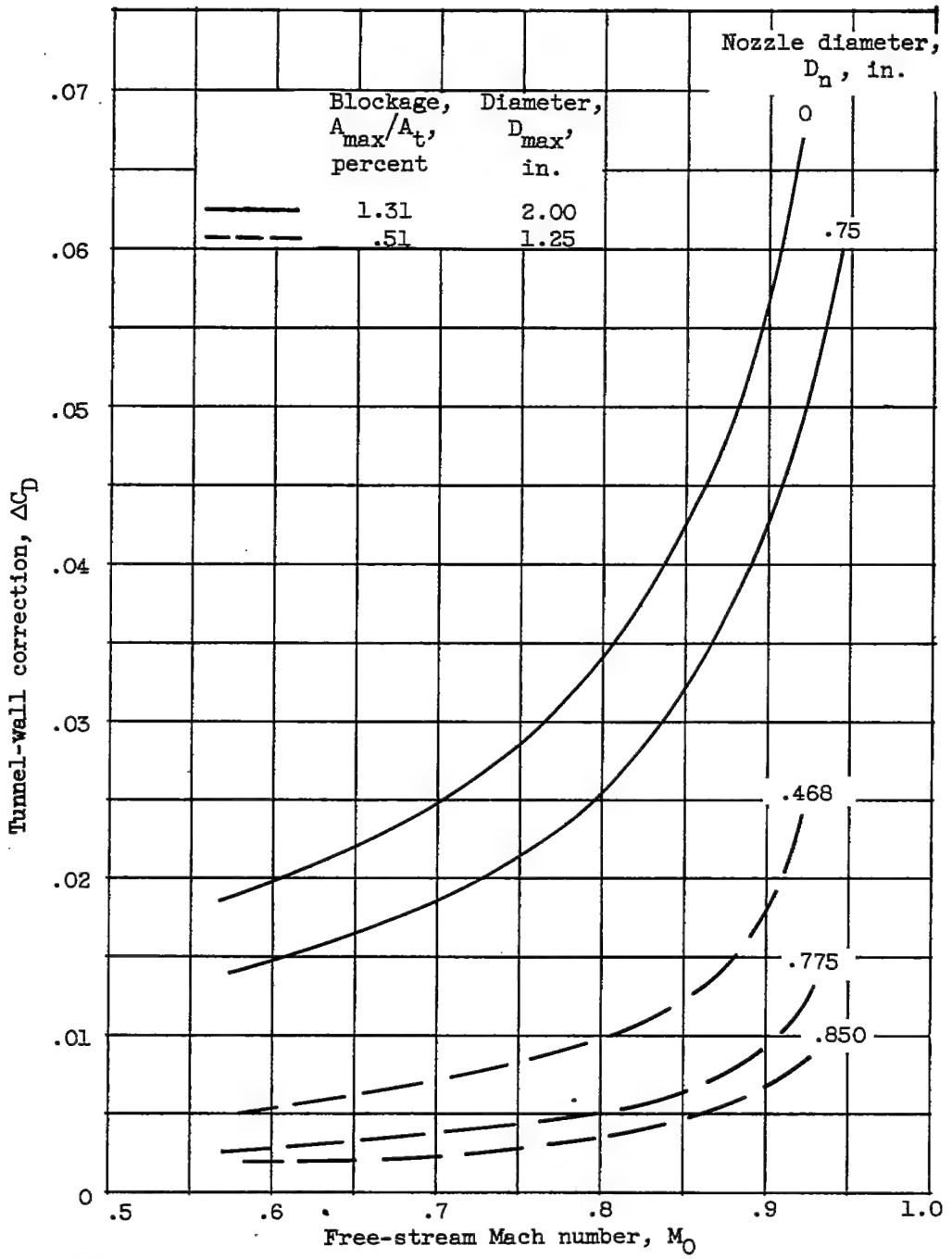

Figure 4. - Wind-tunnel-wall corrections. ($C_D = C_{D,\ measured} + \Delta C_D$.)

[redacted]

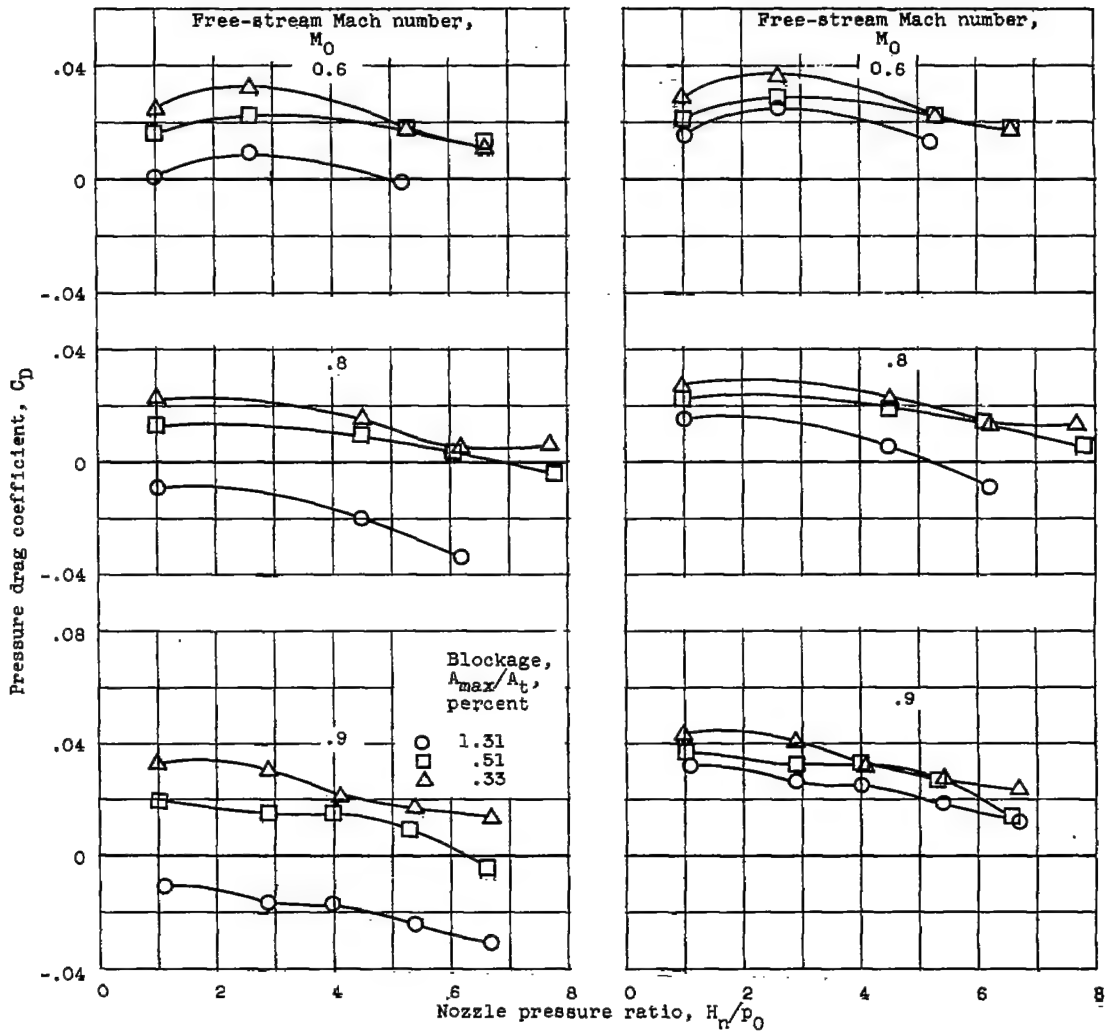

(a) Uncorrected data. (b) Corrected data.

Figure 5. - Blockage model data showing effect of drag corrections.

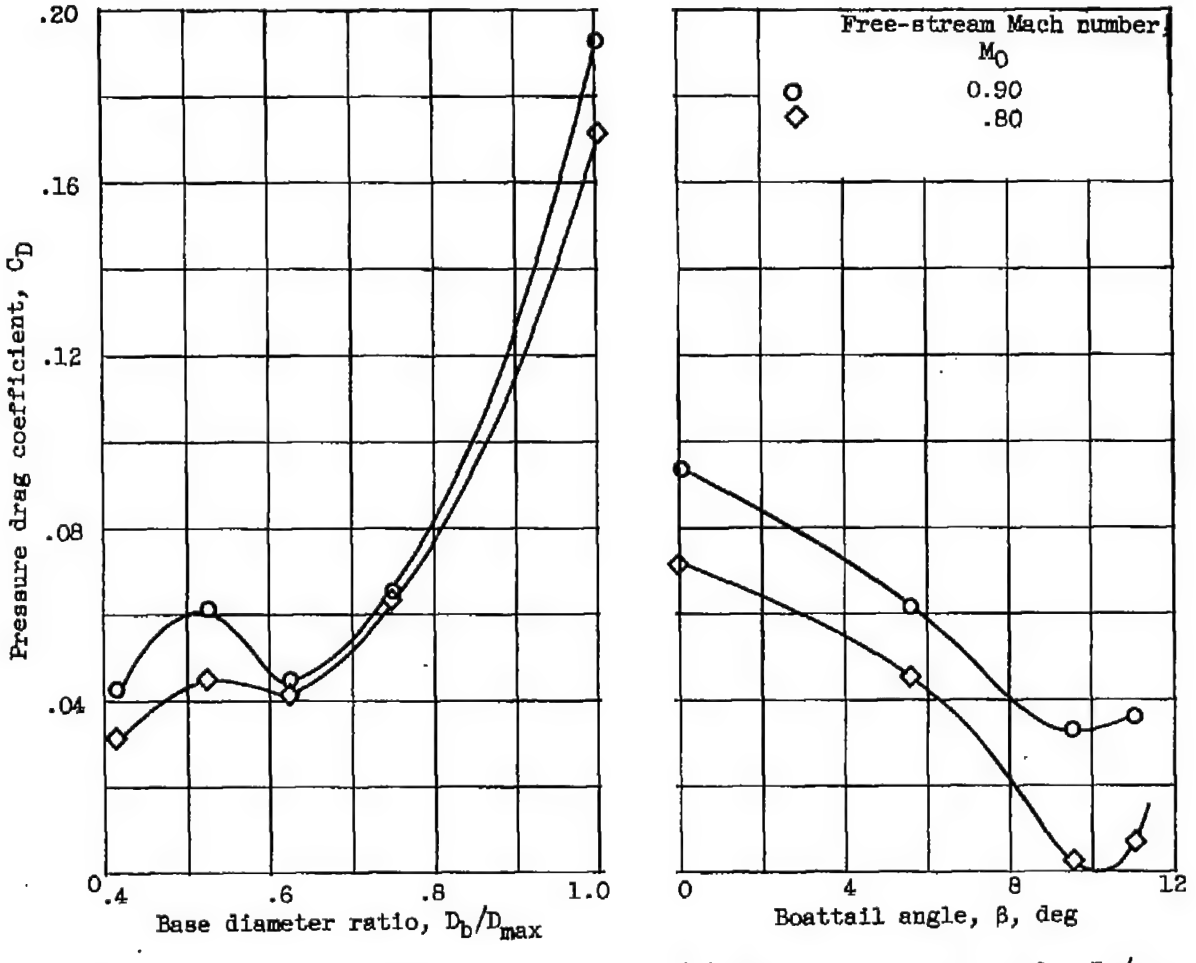

(a) Effect of base diameter ratio; boattail angle, 5.63°.

(b) Effect of boattail angle; D_b/D_{max}, 0.525.

Figure 6. - Effect of boattailing on afterbody pressure drag of blunt-base bodies.

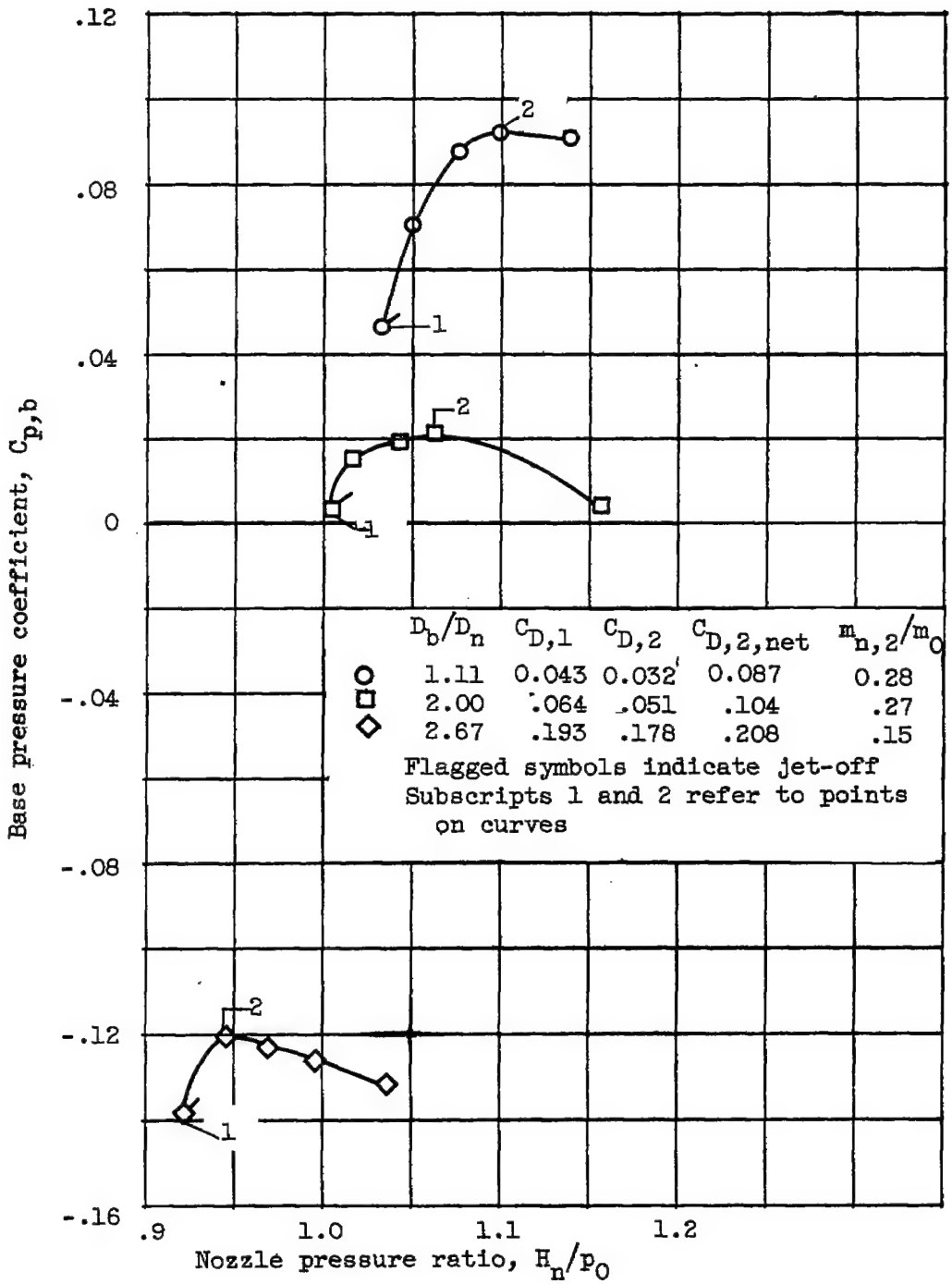

Figure 7. - Effect of base bleed on base pressure coefficient at Mach 0.9.

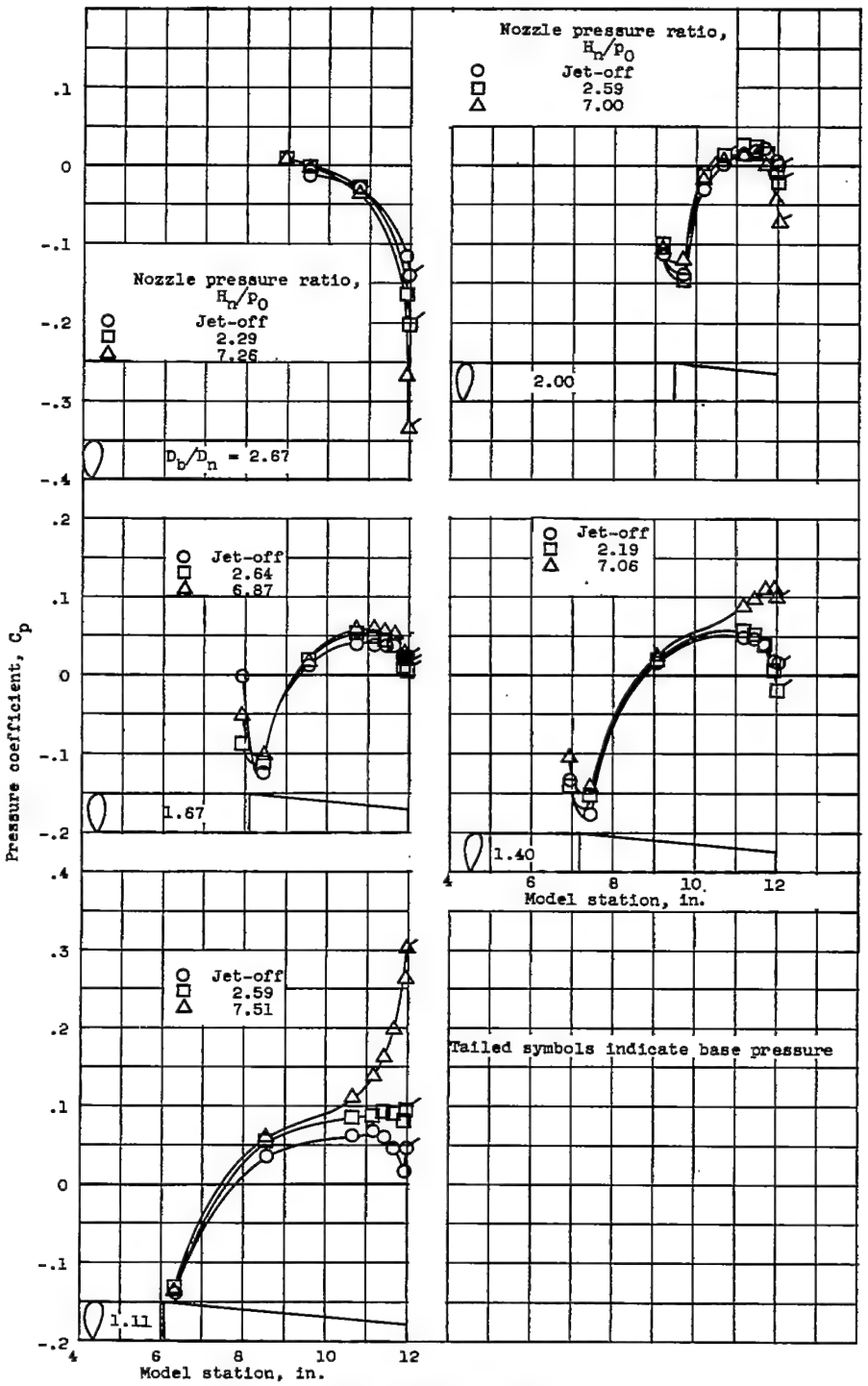

(a) Constant boattail angle, 5.63°.

Figure 8. - Effect of jet on pressure distribution over conical afterbodies at Mach 0.9.

[redacted]

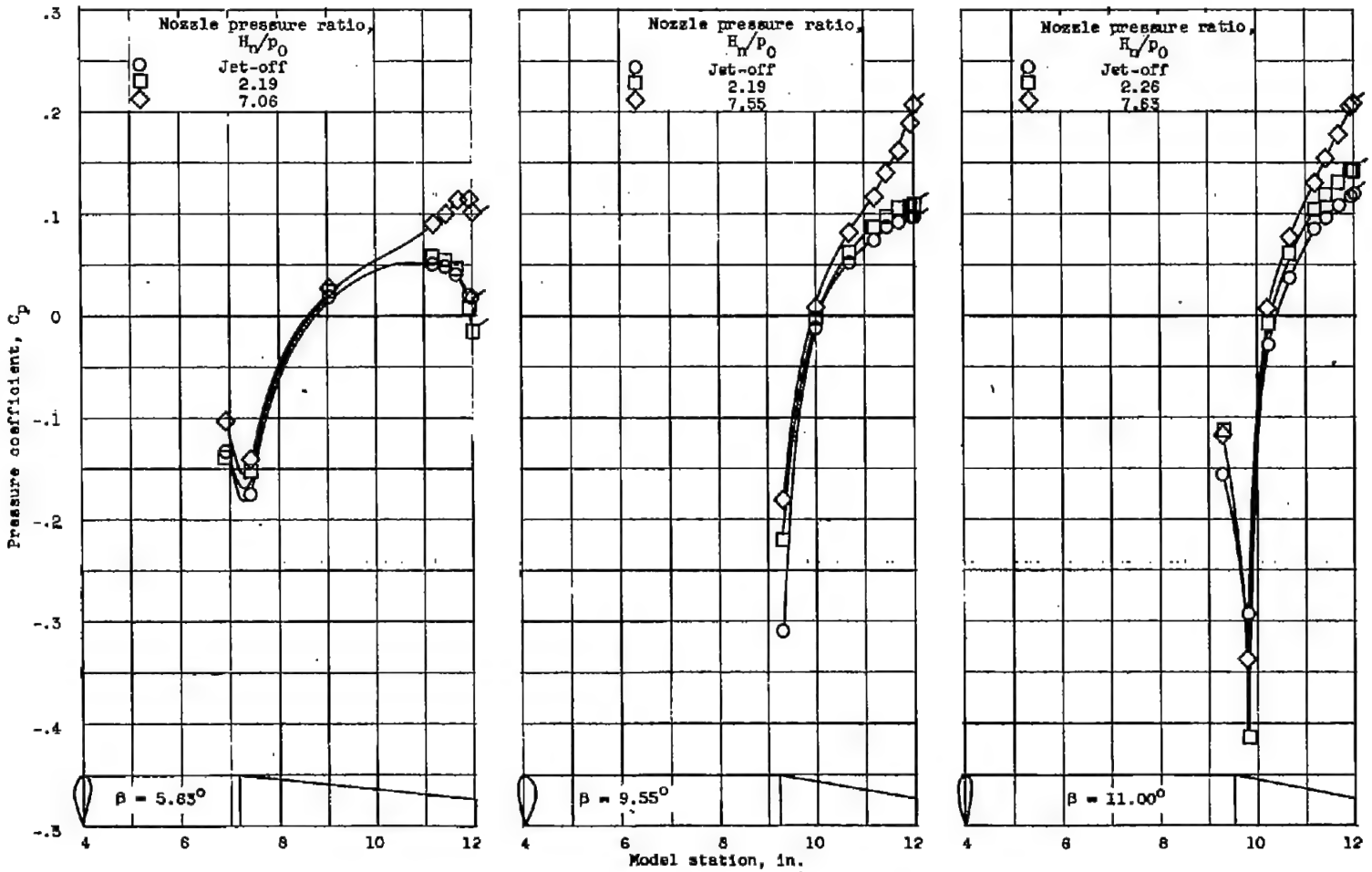

(b) Constant base diameter ratio, D_b/D_{max}, 0.525.

Figure 8. - Concluded. Effect of jet on pressure distribution over conical afterbodies at Mach 0.9.

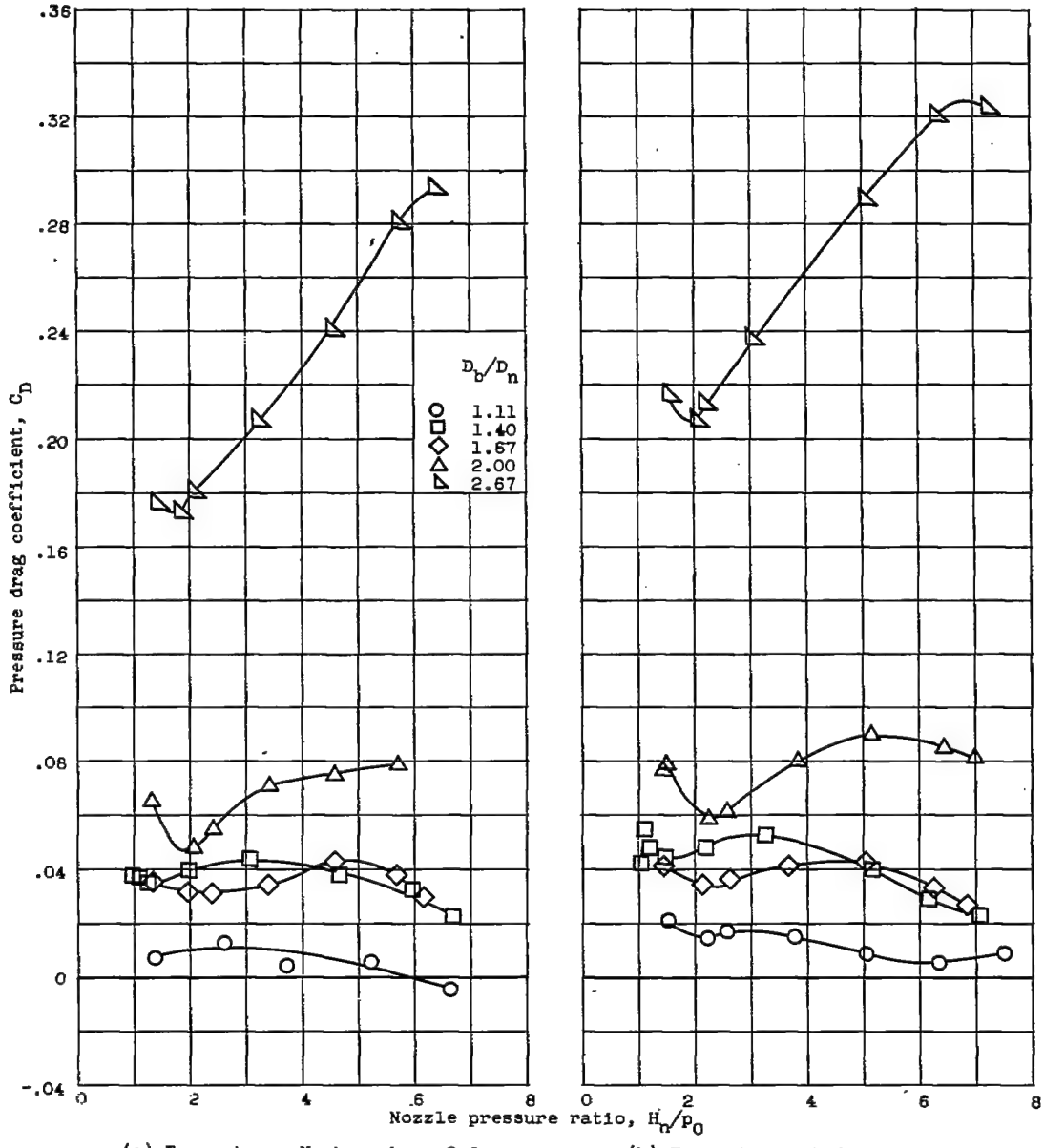

(a) Free-stream Mach number, 0.8. (b) Free-stream Mach number, 0.9.

Figure 9. - Effect of jet on drag of conical afterbodies. Boattail angle, 5.63°.

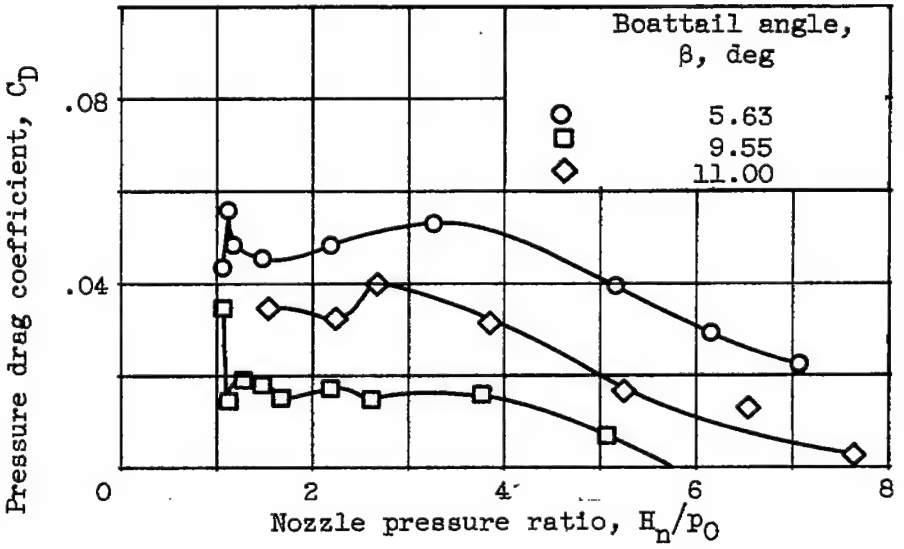

Figure 10. - Effect of jet on drag of conical afterbodies. Free-stream Mach number, 0.9; D_b/D_n, 1.40.

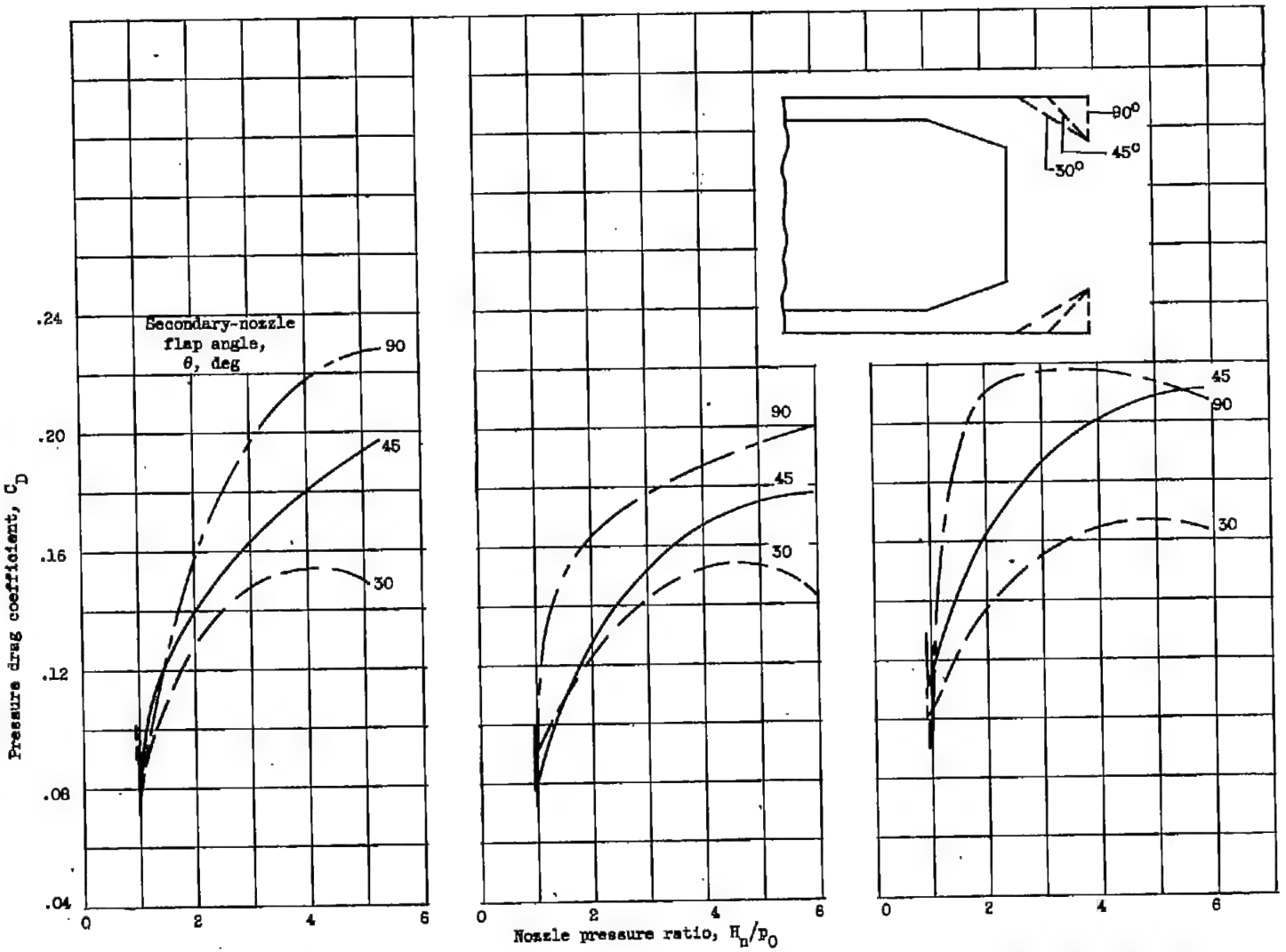

(a) Free-stream Mach number, 0.6. (b) Free-stream Mach number, 0.8. (c) Free-stream Mach number, 0.9.

Figure 11. - Effect of jet on external pressure drag of nacelle-type afterbodies. No secondary flow; A_s/A_{max}, 0.384; D_s/D_p, 1.094.

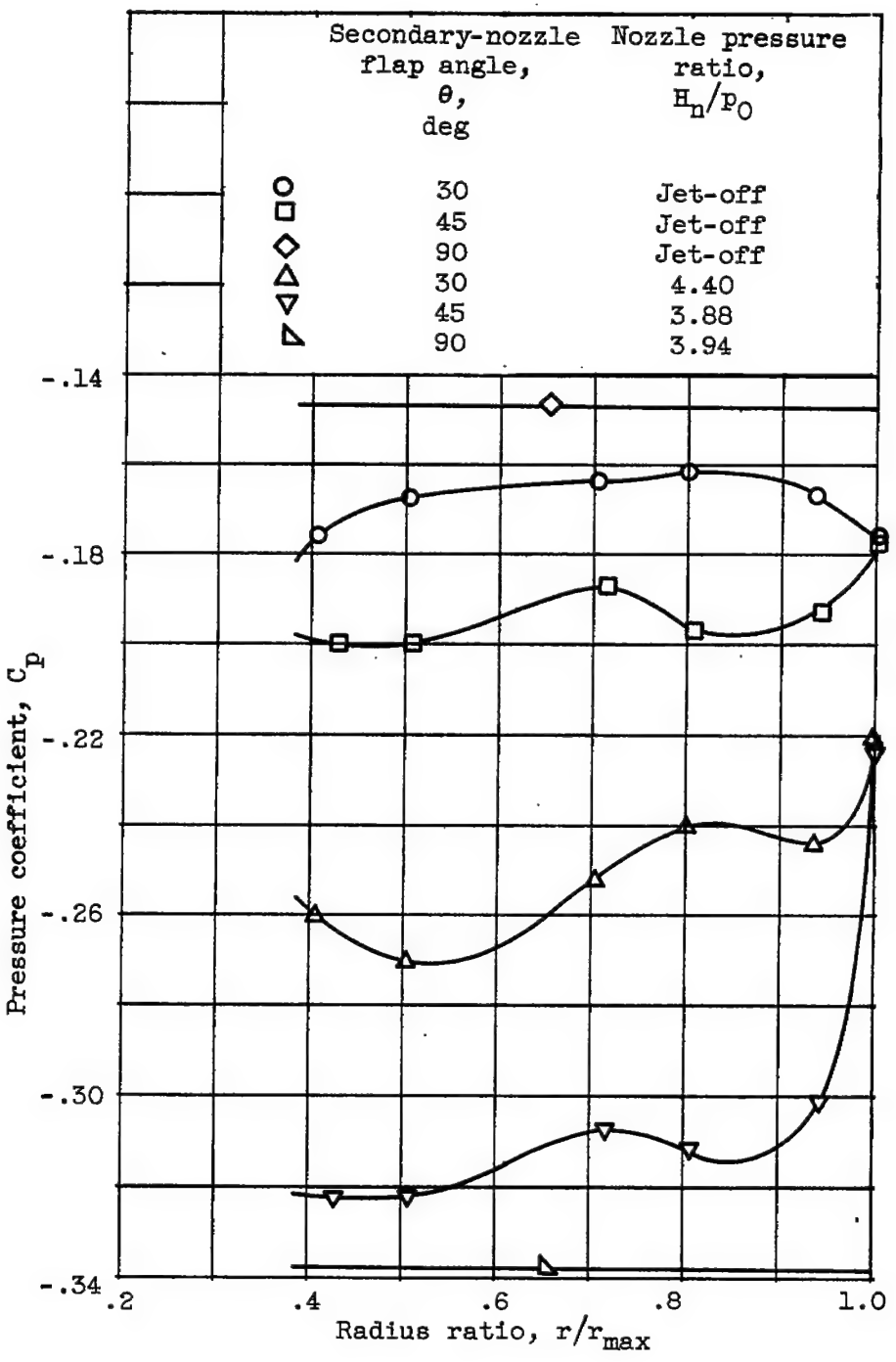

Figure 12. - Pressure distribution over flaps of nacelle-type ejector configurations. Free-stream Mach number, 0.9.

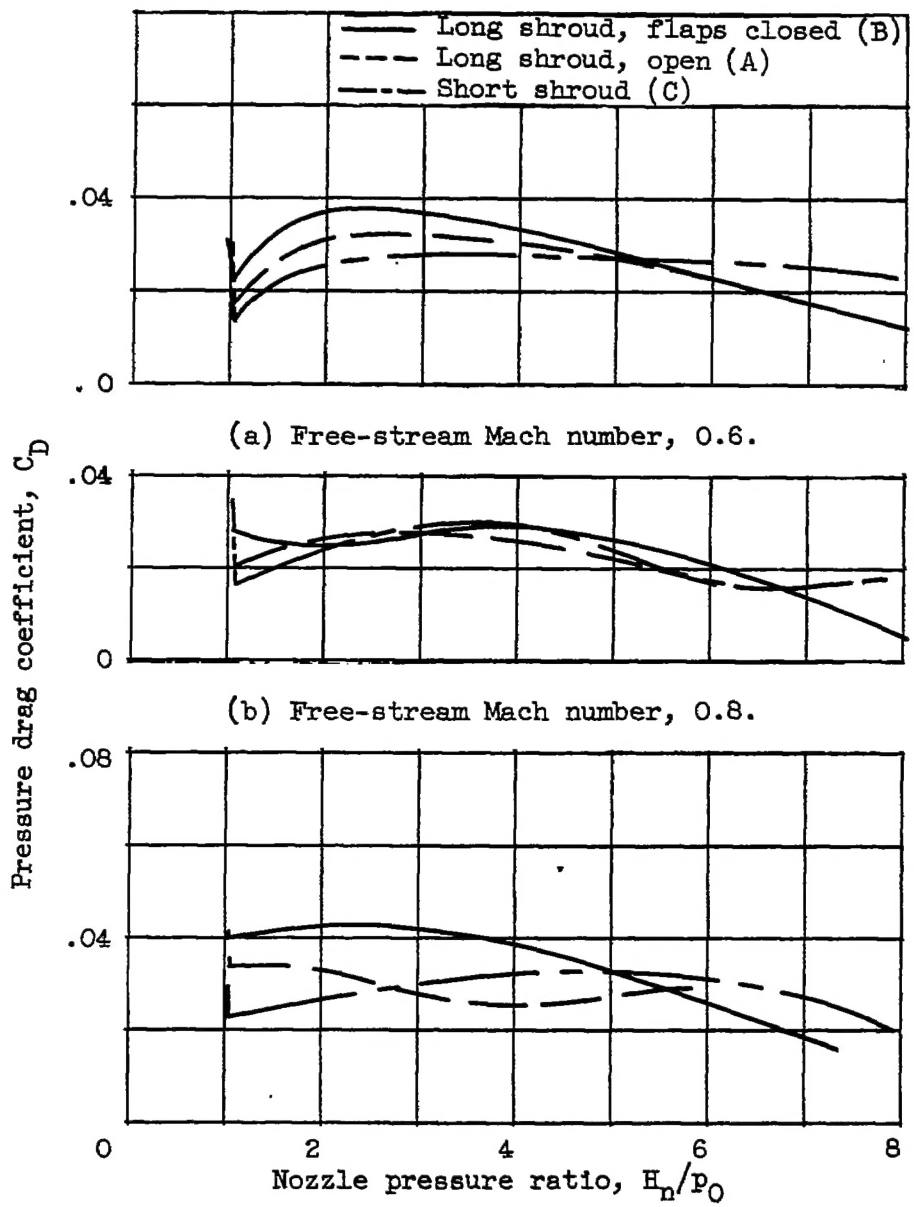

Figure 13. - Effect of jet on external pressure drag of fuselage-type ejector configurations. No secondary flow.

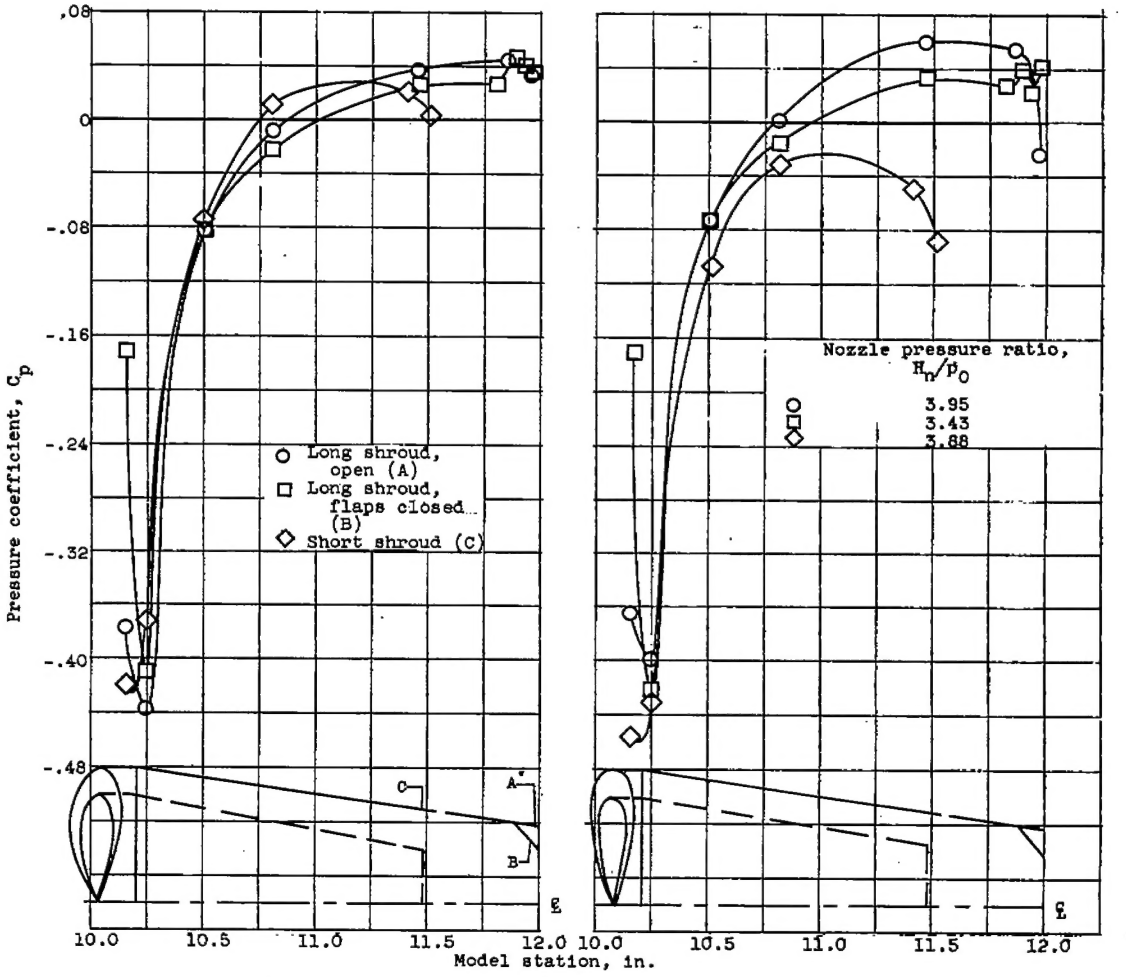

(a) Jet-off (b) Primary flow only.

Figure 14. - Pressure distributions over fuselage-type ejector afterbody configurations. Free-stream Mach number, 0.9.

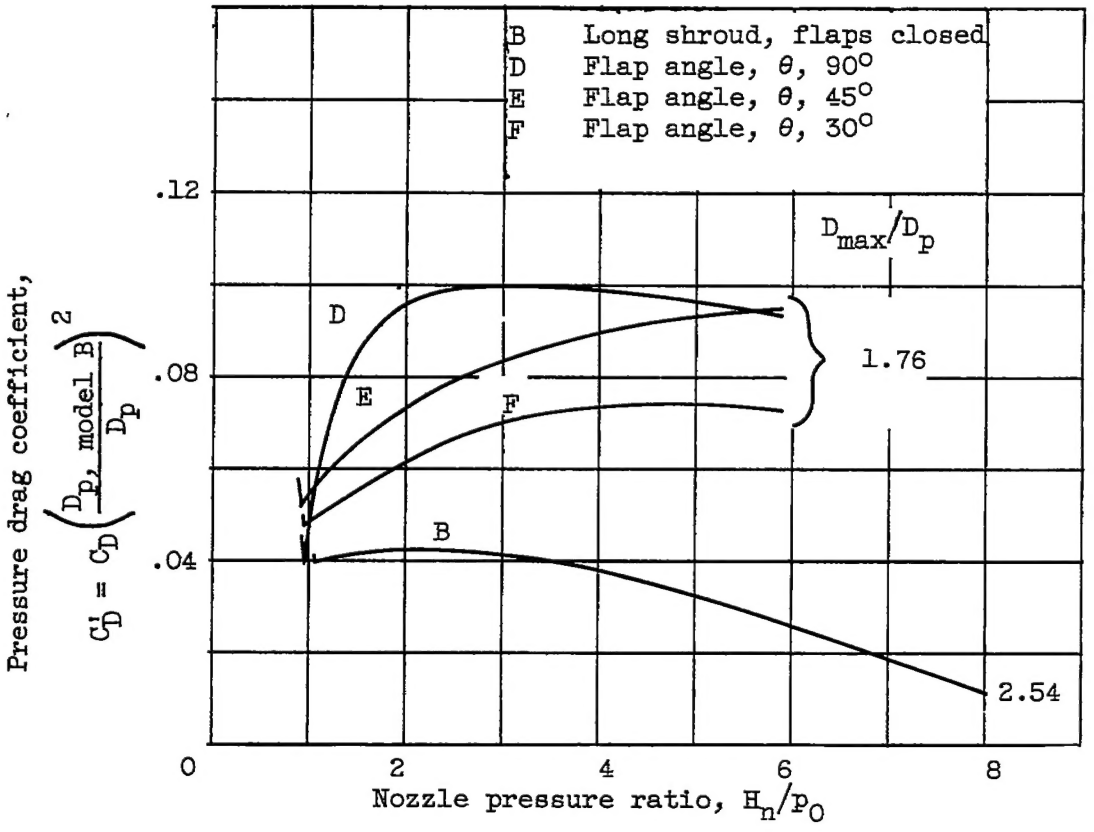

Figure 15. - Comparison of external pressure drag of various ejector configurations with equal primary-jet diameters. Free-stream Mach number, 0.9.

[redacted]

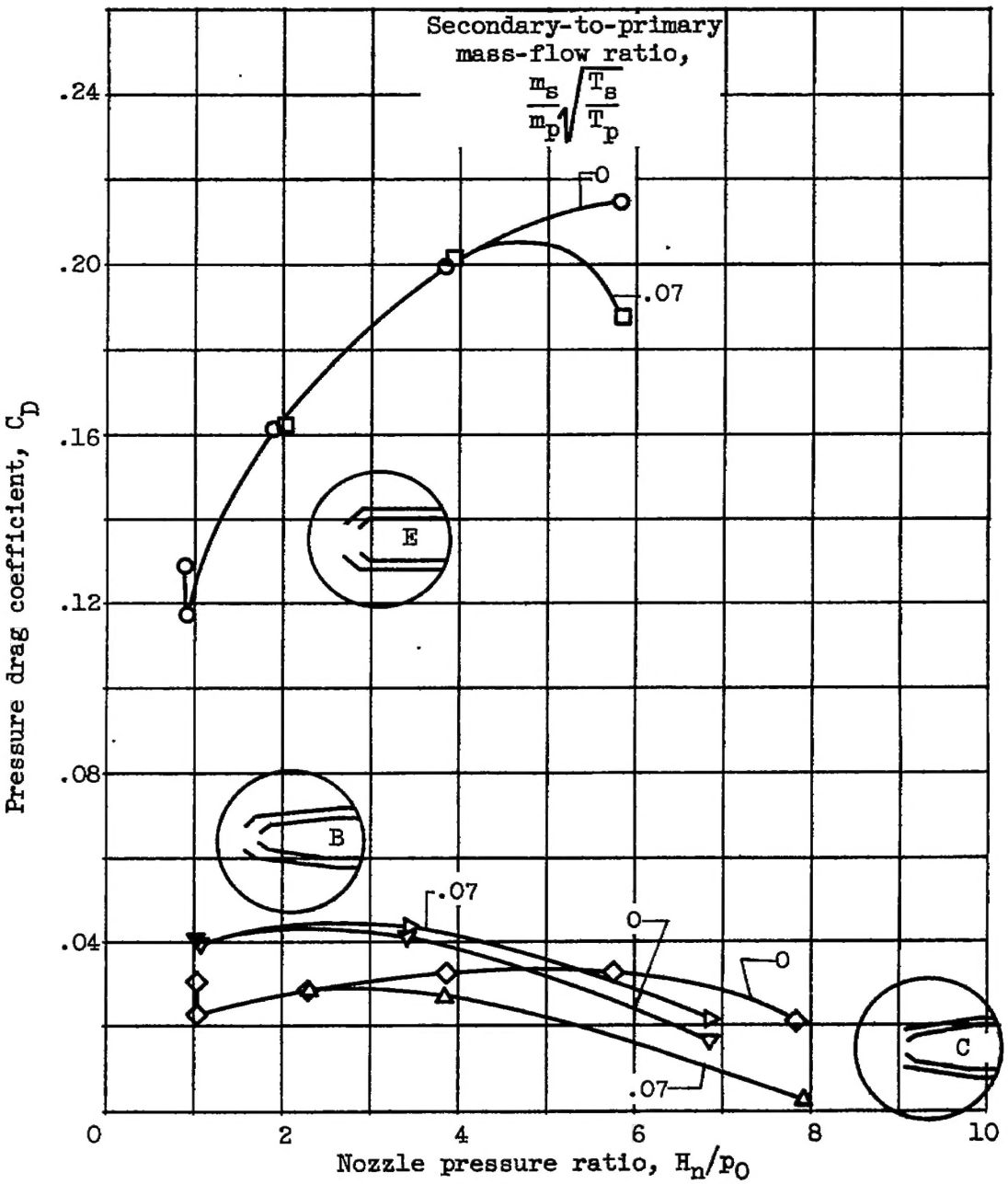

Figure 16. - Effect of secondary flow on external afterbody pressure drag at free-stream Mach number of 0.9.